LONG-TERM BEHAVIOUR ANALYSIS OF RECYCLED ELASTOMERIC MATERIAL FOR HIGH DAMPING VIBRATION LEVELS INDUCED BY RAILWAYS

S. Diego[a], J. A. Casado[a*], I. Carrascal[a], D. Ferreño[a], J. Cardona[b] and R. Arcos[c]

[a] *Materials Science and Engineering Lab. (LADICIM), University of Cantabria, Spain*
[b] *AV Ingenieros, Barcelona, Spain*
[c] *Acoustical and Mechanical Engineering Lab. (LEAM), Polytechnic University of Cataluña, Spain*
*jose.casado@unican.es

Keywords: recycled elastomer, finite elements method (FEM), Insertion Loss, mechanical fatigue

Abstract

The use of elastomeric particles obtained from old tires to produce anti-vibration mats to reduce vibrations in railways is studied. In the first part of this work a numerical simulation for dimensioning the element has been performed. The behavior for a wavy surface was deducted obtaining good approximation to the empirical results. In the second part the methodology used to assess the Insertion Loss, IL, provided by the anti-vibration system is described. The analytical superstructure/ground model developed within the frame of the project is presented. The model is based on an elementary superstructure model with no elastomeric material and is conveniently modified to introduce an under ballast mat. Finally the study shows the validation of the mechanical behavior of prototype mats under dynamic efforts according to standards [1-6]. The results show that the behavior of crushed rubber is suitable to be used as anti-vibration systems.

1. Introduction and aim

Currently there are large accumulations of end-of-life tires in uncontrolled landfills, which generate high environmental impact (Figure 1). The aim of this work is to demonstrate that a respectful environmental elastomeric material, that is prepared based on the mixture of end-of-life tires crushed and resin to be manufactured as mats, can achieve the requirements to reduce vibrations imposed by Railway Administrations. The elastomeric mats can provide an attenuation of the induced ground-borne vibration levels up to 20 dB [1]. If the material is validated for this application, it would be possible to reach a revaluation of 1.5 M of tires in 10 years.

Figure 1. Environmental impact by end–of–life tires [7]

2. Material tested

Anti-vibration mats used for this work were produced by mixing pressure tire granulates out of use from light and/or heavy vehicles characterized previously to be linked with a polymer matrix resin. The design of the mat, in thickness and shape, is determined by stiffness simulations and vibratory studies particularized to the needs of the track. The FEM numerical simulation was carried out considering a thickness of 35 mm, flat geometry on both sides, and flat geometry on top and wavy on the bottom side (see Figure 2). Furthermore, the vibrational and dynamic characterization studies were specifically performed on flat mats. The dimensions of the surface of the mats to perform

reduced scale tests on an universal testing machine, were (300x300) mm^2, while two abutting mats whose dimensions were (1000x500) mm^2 were used to execute the fatigue test on the bench.

Figure 2. Wavy and flat geometries with contact surface (300x300) mm^2

3. Theoretical methodology

3.1. FEM Study

The mechanical response of this kind of materials is usually very complex. Nevertheless, theoretical models to describe the behaviour of non linear elastomeric materials can be found in the literature [8]. In this work, the most relevant models have been evaluated by fitting their material parameters from the experimental information, in order to select the most representative one. The usefulness of this result is evident: after selecting a model and obtaining its parameters, the behaviour of the material is perfectly known and, for example, the in-service conditions could be checked by means of a Finite Elements model. The main mechanical characteristic that defines an elastomer is the ability to withstand great elastic elongations, recoverable after unload. Most of the elastomers show small compressibility and are, in general, known as hyperelastic materials. On the other hand, among the rubberlike materials, the elastomeric foams can be distinguished because they manifest a highly compressible character. In both cases, since the long molecular chains are randomly oriented, the material is initially isotropic. Hyperelastic (or Green-elastic) materials [8] are those for which a strain-energy (per unit of non-deformed volume) potential function exists, being a scalar function of the strain tensor components, $U=U(E_{ij})$. The components T_{ij} of the stress tensor can be expressed according to expression (1). This definition is independent of the compressibility of the material, thus it includes either hyperelastic or elastomeric foams. The bibliography provides several expressions for the strain energy potential, U. In the case of isotropic materials, the models can be expressed in terms of the strain invariants (together with material parameters to be fitted from experimental information. Each model includes a set of material parameters which are, in principle, unknown. They can be evaluated from empirical results coming from mechanical characterisation tests. The Finite Elements software ANSYS [9] is provided with a set of theoretical models with the shape (2); moreover, it includes the tools to evaluate the models from the tests by fitting the unknown parameters. The material constants are determined through a least-squares-fit procedure which minimizes the relative error in stress, RE. For the n nominal-stress-nominal-strain data pairs, the relative measure RE, given in (2), is minimized.

$$T_{ij} = \frac{\partial U(E)}{\partial E_{ij}} \qquad (1)$$

$$RE = \sum_{i=1}^{n} \left(1 - \frac{T_i^{th}}{T_i^{test}} \right)^2 \qquad (2)$$

T_i^{test} being a stress value from the stress data, and T_i^{th} the value coming from the nominal stress expression evaluated. ANSYS [9] minimizes the relative error, E, rather than an absolute error measure since this provides a better fit at lower strains. The following models were analyzed in this work: Mooney-Rivlin, Polynomial, Yeoh, Neo-Hookean, Ogden, Arruda-Boyce, Gent, Blatz-Ko and Ogden hyper-foam. In a preliminary stage of the research the reliability of these models was compared. For this purpose, a compressive test was performed on a flat-type mat which was latter used to fit the free parameters of the above mentioned models. Then, the results were compared through the RE parameter. It was found that the model that best reproduces the behavior of the

material is the five-parameters Mooney-Rivlin which responds to the following equation (3) for the potential energy of deformation:

$$U = c_{10}(\bar{I}_1 - 3) + c_{01}(\bar{I}_2 - 3) + c_{20}(\bar{I}_1 - 3)^2 + c_{11}(\bar{I}_1 - 3)(\bar{I}_2 - 3) + c_{02}(\bar{I}_1 - 3)^2 + \frac{1}{d}(J-1)^2 \qquad (3)$$

where c_{10}, c_{01}, c_{20}, c_{11} and c_{02} are the five free parameters of the Money-Rivlin model, $d = \left(\frac{1-2\cdot nu}{c10+c01}\right)$, nu is the material Poisson's ratio and $\bar{I}_1$ and $\bar{I}_2$ represent, respectively, the first and second deviatoric strain invariants. The fitting parameters obtained for this model are the following: c_{10} = -1.0610, c_{01}= 1.1220, c_{20} = 114.4913, c_{11} = -265.8181 and c_{02} = 156.0450.

3.2. Elastomeric mat's vibration design

The developed superstructure model, considered as a 2-layer continuously supported model where the rail is assumed to be an Euler-Bernoulli beam [11], takes into account the two excitation types that appear in railway systems [10]: quasi-static excitation, caused by the static component of axle loads moving along the track, and dynamic excitation, due to the spatial variation of the support stiffness along the track as well as wheel and rail roughness. Figure 3 shows an outline of this model, where z_r, z_s and z_g are the rail, sleepers and soil displacements, respectively, k_f, k_b and k_{bm} are the fastening, ballast and under-ballast mat stiffnesses, c_f, c_b and c_{bm} are the fastening, ballast and under-ballast mat viscous dampings, and m_b is the ballast mass. Stiffness, damping and sleepers mass are continuously distributed parameters along the track.

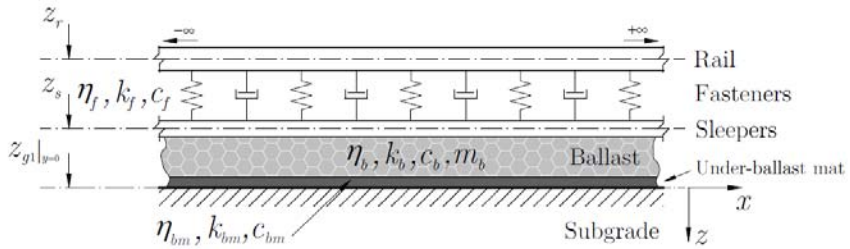

Figure 3. Outline of the considered superstructure model, which includes the under-ballast mat.

Governing equation for the vertical track displacement, z_r, due to wave propagation along it is as Equation (4) [12] shows while, as can be deduced from Figure 3, the distributed force due to sleepers can be described by Equation (5), the sleeper motion by Equation (6) and the force applied for the sleepers onto the soil (superstructure-soil coupling force) can be expressed as Equation (7).

$$EI\frac{\partial^4 z_r}{\partial x^4} + \rho S\frac{\partial^2 z_r}{\partial t^2} + f(x,t) = q(x,t) \qquad (4)$$

$$f(x,t) = k_F(z_r - z_s) + c_F(\dot{z}_r - \dot{z}_s) \qquad (5)$$

$$k_F(z_r - z_s) + c_F(\dot{z}_r - \dot{z}_s) - k_B(z_s - z_g) - c_B(\dot{z}_s - \dot{z}_g) = m_s\ddot{z}_s \qquad (6)$$

$$f_g(x,t) = k_B(z_s - z_g) + c_B(\dot{z}_s - \dot{z}_g) \qquad (7)$$

In these equations, E is the Young Modulus, I is the rail second moment of inertia, ρ is the rail density, S is the rail cross-sectional area, $f(x,t)$ is the distributed force due to the sleepers, $q(x,t)$ is the distributed force due to the train and m_z is the sleeper mass.

The ground is modelled as a homogeneous and viscoelastic half-space defined by Lamé constants, λ and μ, soil density, ρ, and P and S wave damping, DP and DS, respectively. As Metrikine and Dieterman establish [13], the half-space displacement governing equation, following Figure 4, is as Equation (8)

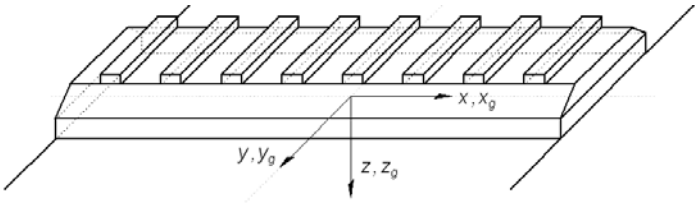

Figure 4. Coordinate system (x,y,z) and soil displacement (x_g, y_g, z_g).

$$(\bar{X}_g, Y_g, Z_g) = (-ik_{x'} - ik_{y'} - v)Ae^{-vz} + \left(-\frac{k_x k_y}{v'}, \frac{k_x^2 - v'^2}{v'}, ik_y\right)Be^{-v'z} + \left(-\frac{k_y^2 - v'^2}{v'}, \frac{k_x k_y}{v'}, -ik_x\right)Ce^{-v'z} \quad (8)$$

Where A, B and C are integration constants that can be calculated from boundary conditions, k_x and k_y are the wave-number in x and y directions respectively, and $k_\alpha^2 = \omega^2/\alpha^2$, $k_\beta^2 = \omega^2/\beta^2$, $\alpha^2 = (\lambda + 2\mu)/\rho$, $\beta^2 = \mu/\rho$, $v = \sqrt{k_x^2 + k_y^2 - k_\alpha^2}$, $v' = \sqrt{k_x^2 + k_y^2 - k_\beta^2}$.

In the other hand, the Insertion Loss, IL, is the parameter used to define the difference of vibration level in a specific location due to the insertion of an elastomeric material. Therefore, the IL will be the parameter used to assess the vibration behavior of the elastomeric mat under study. To perform the IL calculation, the model outlined in Figure 3 (isolated model) and the same model without the elastomeric layer (unisolated model) are used. The receptance of the ground surface at x = 0 m and y = 8 m [6] due to a vertical harmonic load applied on the railhead at x = 0 m is calculated for both unisolated and isolated cases. Each of these receptances has three components $X_{g1}(x,y,\omega)$, $Y_{g1}(x,y,\omega)$, $Z_{g1}(x,y,\omega)$, where x and y are the spatial coordinates according to Figure 3 and ω is the frequency. These three components can be integrated in a global value by the following expressions:

$$U_{g1}^{uniso}(x,y,\omega) = \sqrt{\left|X_{g1}^{uniso}(x,y,\omega)\right|^2 + \left|Y_{g1}^{uniso}(x,y,\omega)\right|^2 + \left|Z_{g1}^{uniso}(x,y,\omega)\right|^2} \quad (9)$$

$$U_{g1}^{iso}(x,y,\omega) = \sqrt{\left|X_{g1}^{iso}(x,y,\omega)\right|^2 + \left|Y_{g1}^{iso}(x,y,\omega)\right|^2 + \left|Z_{g1}^{iso}(x,y,\omega)\right|^2} \quad (10)$$

Setting x = 0, the *IL* is calculated for any distance to the track y using Equation (16):

$$IL = 20log_{10}\left(\frac{U_{g1}^{uniso}(0,y,\omega)}{U_{g1}^{iso}(0,y,\omega)}\right) \quad (11)$$

4. Experimental mechanical characterization

4.1. Static and dynamic modulus (C_{est} and C_{est}) characterization

The mechanical characterization of the mat is performed according to [1-6]. A testing machine with a load cell of ±100 kN, is used to determine C_{est} and C_{est}. This machine has two steel plates (300x300) mm^2 and a ball joint. Strain measurements are performed by four LVDT. C_{est} is determined between 0.02 to 0.10 N/mm^2. To determine C_{din} at 5 Hz the stress measurements are performed between 0.02 and 0.10. C_{est} and C_{din} are obtained as the ratio of the stress variation, $\Delta F/S_0$, and the average shortening of the mat, $\Delta\delta_m$, according to expression (12):

$$C_{est\ or\ din} = \frac{\Delta F}{S_0 \cdot \Delta\delta_m}\ (N/mm^3) \quad (12)$$

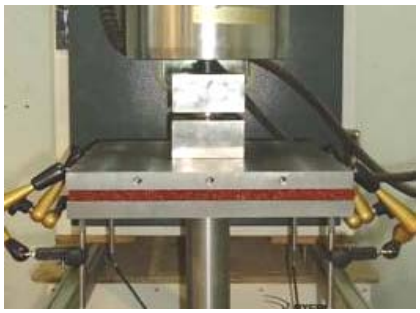

Figure 3. Device used in the tests

4.2. Fatigue test

The fatigue test is performed on an area of 1 m^2 mat according to [5]. The sample, which has a longitudinal joint in the center, is supported on a steel plate into a wooden drawer. The total test surface of the sample is covered by a geotextile to prevent damage by punching ballast. Then the drawer is filled with ballast up to reach a height of 35 cm. A steel disc 600 mm diameter to distribute the loads is placed on the ballast (see Figure 4). For this test, the loads are 10 kN for the minimum level and 56 kN for the maximum during 10^7 cycles at 5 Hz. In the next level, the maximum load is increased up to 75 kN, this second phase lasts $2.5 \cdot 10^6$ cycles. C_{est} measurements are performed without ballast before and after testing. Also static and dynamic measurements are taken along the test with ballast. A bench equipped with a servo-hydraulic actuator with a load cell of ±100kN was used. The displacements are measured by four LVDT. C_{est} variation due to fatigue conditions is determined after the test. C_{est} is measured with the sample located between the steel plate and the loading disc (Figure 5) by applying a stress between 0 and 0.11 N/mm^2 at 1 mm/min. Then C_{est} is calculated in the range from 0.02 N/mm^2 to 0.1 N/mm^2 using expression (10).

Figure 4. Fatigue test device

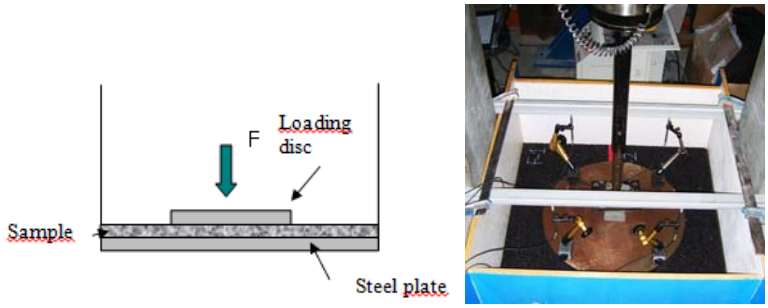

Figure 5. Arrangement C_{est} test before and after fatigue test

5. Results and analysis

5.1. FEM Analysis

Once the free parameters of the Mooney-Rivlin material were calibrated, this information was used to build a FE of an wavy mat. The purpose of this stage is to validate the numerical technique. Figure 6 provides an overview and a detail of the meshing of the wavy mat. In this case the

geometrical irregularities forces to use tetrahedron type elements HYPER158, compatible with the Mooney-Rivlin material model, for the mesh. As a rule of good practice, the mesh density was increased in the regions of contact. The boundary conditions of the test have been imposed by modeling the supports and the load applier as rigid elements, with their corresponding contacts; TARGE170 elements were used for this purpose. The influence of several variables was analyzed.

First, a study of the influence of the size of the element used in the mesh was conducted. As a result, an element size of 12 mm was chosen, because without producing too computationally expensive calculations, it provides satisfactory results. Moreover, the so-called convergence factor which defines the contact stiffness was studied. The convergence calculation is improved by reducing its value but, in return, the calculation is less precise. A trade-off must be found, therefore. Thus, the suitable value $3 \cdot 10^{-5}$ was chosen for the convergence factor. Figure 7 shows a comparison between the experimental results (two loading-unloading compression tests, Exp_1 and Exp_2, performed on a wavy type specimen) and the numerical model predictions.

As can be seen, the level of agreement is really satisfactory. Thus, in the loading ramp a virtually perfect overlap between the experimental curves and the numerical predictions can be observed. Therefore it can be said that the latter has been validated by the empirical results. It is worth noting that the definition of the model used for the simulations imposes certain limitations on the representativeness of the results. Thus, such models are unable to take into account the dissipative phenomena occurring in the material subjected to loading-unloading processes which are responsible for the hysteresis phenomena observed. It is therefore not possible to predict the behavior of the material during the unloading stage. However, this does not spoils the usefulness of the finite element model to characterize the behavior of the mats because, as explained in the text, their stiffness is determined using only the loading ramps of the experimental curves [1].

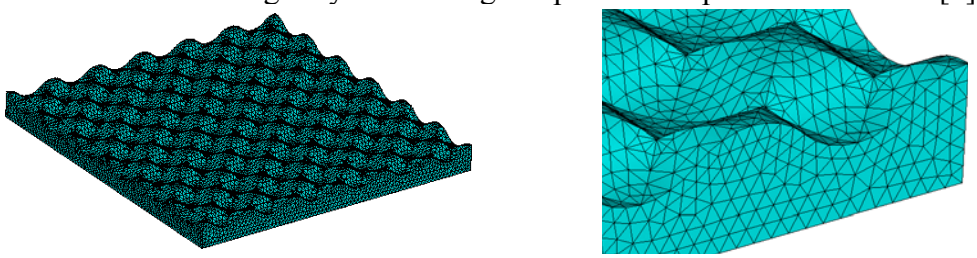

(a) (b)

Figure 6. Overview (a) and detail (b) of the meshing of the wavy mat

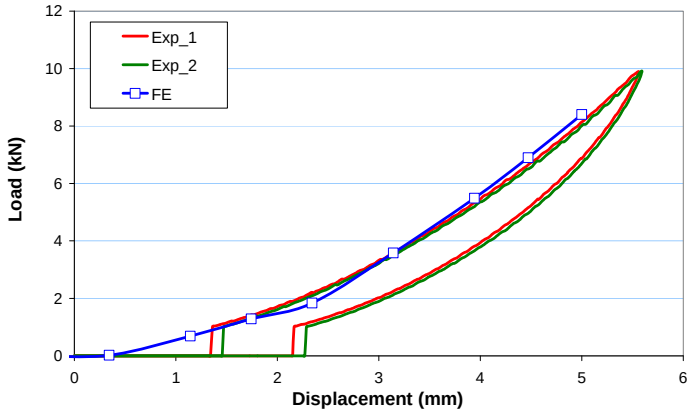

Figure 7. Comparison between FE predictions and experimental results

5.2. Ground vibration level reduction

Insertion Loss, *IL*, calculation as a function of frequency in the range 1-80 Hz at different distances *y* from the track using the methodology previously described, are shown in Figure 8. In order to take into account the whole range of possible soils, in this figure the UBM *IL* is calculated for two types of soils: one representing a soft soil (50 MPa) and another one representing a stiff soil (300 MPa).

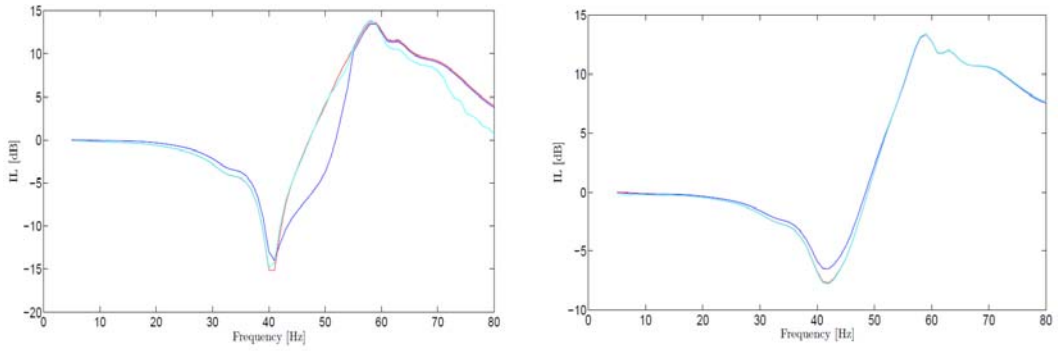

Figure 8. IL prediction UBM at y = 2 m (dark blue), y = 8 m (red) and y = 15 m (light blue) on a) soft soil and b) stiff soil.

5.3. Mechanical Characterization

Throughout the fatigue test C_{est} with ballast has been calculated between 0.02 N/mm^2 and 0.1 N/mm^2. Periodic determinations of C_{din} were performed throughout the test. Figure 9 shows that C_{din} does not stabilize until $5 \cdot 10^6$ cycles, and a further increase is found when the 2nd phase starts. Figure 10 shows the stiffening suffered by the system from the results observed in the static tests performed at the beginning (initial), middle ($5 \cdot 10^6$ cycles), at the end of the 1st phase (10^7 cycles) and at the end of the 2nd phase ($12.5 \cdot 10^7$ cycles). Analyzing the evolution of the assembly´s stiffness, mat and ballast, the variations between the initial and final values are very high, both in dynamic and static regime. After the test, ballast and geotextile are removed and the static test on the mat is repeated. Figure 11 shows the C_{est} variation experimented by the mat after $12.5 \cdot 10^6$ cycles. The behavior of the mat reflects smoother stiffening (10%). These data indicate that the greater mechanical damage suffered by the system, corresponds to the ballast, keeping the results for the mat in acceptable values.

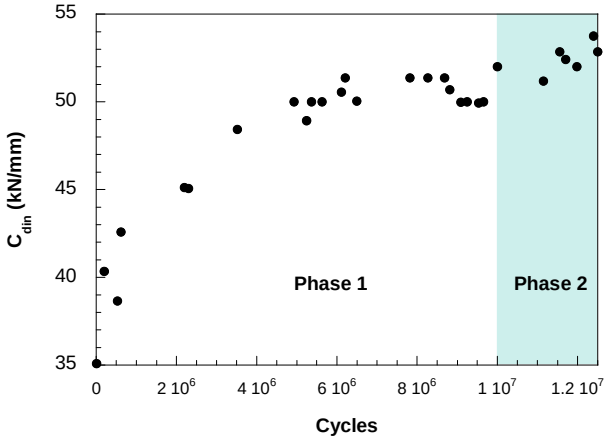

Figure 9. Evolution of C_{din} with ballast

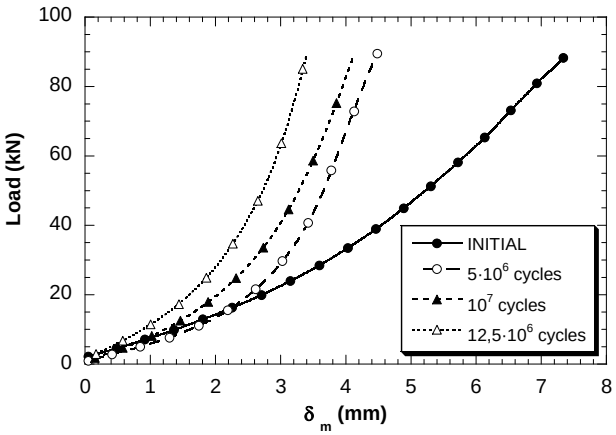

Figure 10. Evolution of C_{est} with ballast

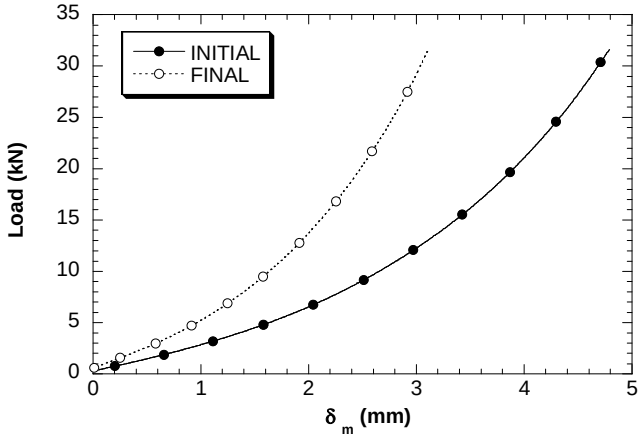

Figure 11. Evolution of C_{est} without ballast

6. Conclusions

Refering to the material under study, the dynamic behavior of end-of-life tires blended with polyurethane resin, in the right proportions and the optimal particle size and thickness, is suitable to be used as anti-vibration system for railway applications.

High variations were verified in the measurements made on the ballast–mat system, in dynamic conditions and, even more pronounced, under static conditions. However, the measurements performed on the mat without ballast after the fatigue test showed variations of only 10%. That fact evidences that the ballast is the part of the system more deteriorated.

Regarding to the numerical aspects, in this paper a finite element numerical model suitable of reproducing the mechanical behaviour of the mats characterized was developed and experimentally validated. For this, first, the representativeness of a series of appropriate mechanical behaviour models for hyperelastic and elastomeric materials was contrasted.

The experimental data (obtained from flat mats) allowed the five-parameters Mooney-Rivlin model to be selected as the most appropriate. Once its free parameters were identified, a FE model of the wavy-mats was generated. By comparing the numerical predictions and the experimental results it was possible to validate the model. This result lets to replace laboratory tests by numerical simulations to characterize the behavior of mats with different geometries simplifying the process.

Regarding the mat's vibration isolation behaviour, a predictive 2-layer continuously supported superstructure/ground model has been developed. Calculations for two soil's type show an acceptable efficiency in terms of vibration isolation, considering the Insertion Loss, IL, parameter.

Acknowledgements

This work has been performed in the frame of the RECYTRACK project, reference LIFE 10 ENV/ES/000514, in collaboration with Acciona Infraestructuras, Adif, AV Ingenieros and Ladicim. The financial support of the Europ Commission through LIFE+ instrument is kindly acknowledged.

References

[1] Pliego de Prescripciones Técnicas Particulares "Contratación del suministro de manta antivibratoria destinada a la línea de alta velocidad noroeste" de ADIF. Abril 2010.
[2] DBS 918 071-01, "Condiciones técnicas de suministro, Acolchado de subbalasto para reducir la carga ejercida sobre el balasto. Ensayos mecánicos".
[3] Especificación Técnica ET-V-C-99-99-0102/6-U00-999, "Manta amortecedora de impacto e vibração do lastro-fornecimento e instalação".
[4] DIN 45673-1:2010-08, "Mechanical vibration. Resilent elements used in railway tracks. Part 1: Terms and definitions, classification, test procedures".
[5] DIN 45673-5:2010-08, "Mechanical vibration. Resilent elements used in railway tracks. Part 5: Laboratory test procedures for under-ballast mats".
[6] UIC CODE 719-1. June 2011. Recommendations for the use of Under Ballast Mats. UBM. 1st edition
[7] http://www.elespectador.com/node/405517
http://lasfotosmasalucinantes.blogspot.com.es/2012/02/vertedero-ilegal-de-neumaticos-en-el.html
[8] L. E. Malvern. Introduction to the Mechanics of a Continuous Medium. Prentice-Hall Inc. N. J. 1969.
[9] ANSYS User's Manual, 2013.
[10] Lombaert, G., Degrande, G. "Ground-borne vibration due to static and dynamic axle loads of InterCity and high-speed trains". *Journal of Sound and Vibration*, **319**(3-5), 1036-1066, (2009).
[11] Knothe, K.L., Grassie, S.L. "Modelling of railway track and vehicles/track interaction at high frequencies". *Vehicle System Dynamics*, **22**(3-4), 209-262, (1993).
[12] Graff, F.G. *Wave Motion in Elastic Solids.* New York, Dover publications Inc., 309-430, (1975).
[13] Metrikine, A.V., Dieterman, H.A., "The equivalent vertical stiffness of an elastic half-space interacting with a beam, including the shear stresses at the beam – Half-space interface". *European Journal of Mechanics A/Solids*, **16**(3), 515-527, (1997).